A Doubly Charged Ion Model for Ion Thrusters

R.R. Peters* and P.J. Wilbur†
Colorado State University, Fort Collins, Colo.
and
R.P. Vahrenkamp‡
Hughes Research Laboratories, Malibu, Calif.

A theoretical equilibrium model of doubly charged ion production and loss processes in electron bombardment ion thrusters is presented. The model is shown to predict double ion density levels accurately for 15- and 30-cm diam thrusters operating with several different grid sets and at several different power levels. The model indicates that the dominant mechanism of double ion production involves the singly charged ground state. This result is used to develop a much simpler model, which, along with correlations of the average plasma properties, can be used to determine the double ion density in thrusters with acceptable accuracy.

Introduction

DOUBLY charged mercury ions, which are observed in the discharge chambers of mercury electron bombardment thrusters, are undesirable because 1) they increase the rate of sputtering damage to discharge chamber components, 2) they complicate the otherwise simple relationship between ion beam current and thrust, and 3) they effect a reduction in overall thruster efficiency. Although it is desirable to reduce the doubly charged ion density, such a reduction should not be accompanied by undesirable side effects such as thruster performance degradations. Identifying the thruster design and operational changes, which yield good thruster performance and low doubly charged ion densities experimentally, would be expected to be time-consuming and costly. The development of an accurate theoretical model should, on the other hand, facilitate the definition of preferred designs quickly and at low cost. It should also enable a designer to determine the effects of changes in design variables. Although the model presented here has been verified experimentally for thrusters that use mercury propellant only, it is considered to be applicable to other propellants if valid cross-sectional data are provided for them.

Theoretical Model

In order to develop a simple model describing the double ion density in the discharge chamber only those ionic and atomic species that were considered significant in determining the double ion density were included. The significant species were selected as those that have substantial electron impact cross sections of formation over the electron energy range of interest, so that large numbers of these excited atoms or ions are produced. These states also were required to have sufficiently long effective lifetimes so that they could participate in production processes before they decayed.

Figure 1 is a discharge chamber reaction schematic showing these dominant species and the reactions in which each species can participate. The symbols used in Fig. 1 represent the following species: Hg^0, neutral ground state mercury; Hg^m, metastable neutral mercury (6^3P_0 and 6^3P_2 states); Hg^r, resonance state neutral mercury (6^3P_1 and 6^1P_1 states); Hg^+, singly ionized ground state mercury; Hg^{m+}, singly ionized metastable mercury ($6^2D_{3/2}$ and $6^2D_{5/2}$ states); and Hg^{++}, doubly ionized ground state mercury.

The arrows in Fig. 1 indicate the various interaction routes considered in this analysis, and three different types of reactions are considered. The first type of reaction, shown by an arrow going from one species to a more highly excited one, occurs when an electron interacts with an atom or ion, producing a more highly excited atom or ion (e.g., the production of double ions from single ions). The production of a highly excited atom or ion also represents a loss mechanism for the less excited species. The analysis assumes that excitation reactions are induced by electrons having the two-group (Maxwellian plus monoenergetic) energy distribution common to mercury ion thruster plasmas.

The second type of process, indicated in Fig. 1 by a dotted line, is that of an atom or ion going to a plasma boundary. Such a boundary either could be the discharge chamber wall on which the atom or ion would be de-excited, or it could be a grid aperture, in which case the atom or ion would be extracted from the discharge region. In either case, this represents a loss rate for any of the excited states. The large arrow back to the neutral ground state represents the resupply of neutral ground state atoms either from the walls or from the propellant supply system.

A third type of reaction shown in Fig. 1 is relevant only to the two resonance states. The resonance states differ from metastable states in that they have a very short lifetime before they de-excite spontaneously by emitting a photon of light. However, the energy of this photon is such that it is absorbed readily by a nearby neutral ground state atom, producing another resonance state atom. Since the transport time of the photon is small compared to the excited state lifetime, the excited state can be considered to exist continuously. Eventually, the photon can diffuse to a boundary, where it will be lost. This is equivalent to the loss of a resonance state atom, and it is represented in Fig. 1 by a dotted line conveying a photon to the wall and a branching line going from the resonance atom to the neutral ground state atom.

At equilibrium, the rate of production of a given species must equal its loss rate, and this fact gives rise to a series of equations containing as dependent variables the density of each species considered in the analysis. Because each species generally is produced from several lesser excited species and because the plasma properties that determine the production rates vary from point to point in the discharge chamber, the production portion of each of these equations is the sum of several volume integrals. Likewise, the loss rate is the sum of several volume integrals corresponding to those losses due to excitation of the species to still higher states and a surface

Presented as Paper 76-1010 at the AIAA International Electric Propulsion Conference, Key Biscayne, Fla., Nov. 14-17, 1976; submitted Nov. 29, 1976; revision received April 11, 1977.
Index category: Electric and Advanced Space Propulsion.
*Presently Member of the Technical Staff, Sandia Laboratories, Albuquerque, N.M. Member AIAA.
†Associate Professor of Mechanical Engineering. Member AIAA.
‡Member of the Technical Staff. Member AIAA.

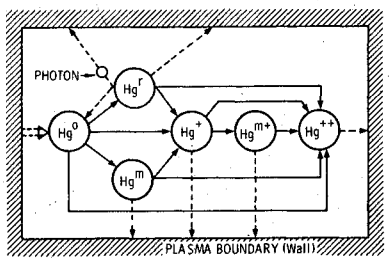

Fig. 1 Discharge chamber reaction schematic.

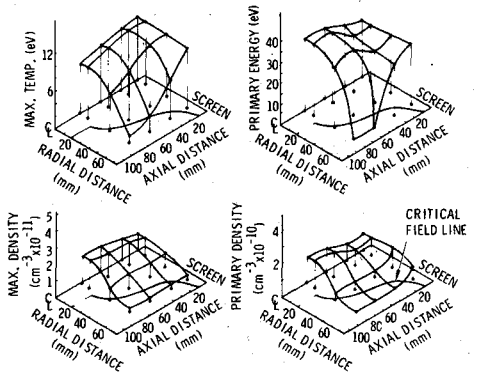

Fig. 2 Plasma property profiles (15-cm thruster, SERT II grids, 37-V anode voltage).

integral representing the loss of the species via migration across the plasma boundary. Examples of these integral equations for several of the species are developed in Refs. 1 and 2.

The bulk of the ion thruster ionization and excitation processes generally occur within the region defined by the surface of revolution of the critical field line[3] and the screen grid, because this region contains most of the electrons that have sufficiently high energies to effect these excitation reactions. Because the plasma is fairly uniform in this region, the integral equations can be converted into algebraic equations written in terms of volume- and surface-area-averaged plasma properties. The volume-averaged plasma properties define plasma conditions appropriate to the bulk of the plasma, whereas the surface-area-averaged properties pertain to the critical field line-screen grid boundary. In this analysis, however, the most important surface-averaged quantities are the single and double ion fluxes, which determine the ion loss rates. These fluxes are expressed in terms of plasma uniformity factors, which are defined as the ratios of the volume-averaged ion flux to the boundary-surface-averaged flux for single and double ions. The development of the equations for properly weighted volume-averaged properties and for the plasma uniformity factors is contained in Ref. 1.

The algebraic production and loss rate equations discussed in the preceding paragraph can be solved to determine the ratio of the density of any given species to the neutral ground state density (i.e., the relative density of the species). The additional requirement that the plasma be neutral implies a relationship between ion and electron densities which enables one to solve uniquely for ground state single, metastable single, and double ion densities. These, in turn, imply a unique neutral atom density and hence a unique density for each species considered in the analysis. One must, however, iterate to arrive at these densities, because a neutral ground state atom density must be assumed initially to determine the photon loss rates.

A computer program has been written which calculates the densities of all the species considered in the model. These densities are calculated by using the relative density equations and plasma neutrality condition mentioned. The input needed to make these calculations includes the volume-averaged plasma properties, the plasma uniformity factors, the volume-to-surface area ratio of the primary electron region, and the relevant cross-sectional data. A complete description of this model is contained in Ref. 1.

Experimental Procedures

The model discussed in the previous section will predict the species densities if the volume-averaged plasma properties, uniformity factors, and geometric quantities, which collectively are called the input parameters, are known. In order to verify the accuracy of this model, these input parameters were measured at essentially the same time as the double-to-single ion density ratio was being determined from mass spectrometer[4] measurements in the ion beam of a thruster. The double-to-single ion density ratio measured in this way then was compared to that calculated from the model using the measured input parameters.

In order to test the accuracy of the model over a wide range of conditions, data were used from different thrusters and operating conditions. The 15-cm diam SERT II thruster was operated with two different grid sets and at three different power levels for each of these grid configurations. Data were collected at each condition, allowing the accuracy of the model to be verified at six different points. Data for the 30-cm diam thruster also were obtained at Hughes Research Laboratories, so that the model could be verified over a wider range of thruster sizes, configurations, and operating conditions. Both thrusters have similar divergent magnetic field configurations, and their specifications and operating characteristics are described in the literature.[5-7]

The "Operating Variables" section of Table 1 lists the operating conditions and accelerator grid configurations used in testing the 15-cm thruster at Colorado State University (CSU) and the 30-cm thruster at the Hughes Research Laboratories. The SERT II grids and the dished grids used on the 15-cm-diam thruster are described in Ref. 5. The EM (engineering model) and SHAG (small hole accelerator grid) grids used on the 30-cm thruster are described in Refs. 8 and 9.

In order to determine the values of the average plasma properties for use in the theoretical model, the primary electron density and energy and the Maxwellian electron density and temperature first were determined at 16 locations in the discharge chamber at each operating condition. These plasma properties were measured using a Langmuir probe, and the resultant data then were analyzed using the procedure described in Ref. 10. The results of a typical survey (15-cm thruster, SERT II grids, 37-V anode voltage) showing the spatial variation in Maxwellian electron temperature, primary electron energy, and primary and Maxwellian electron densities are plotted in Fig. 2. The Maxwellian electron

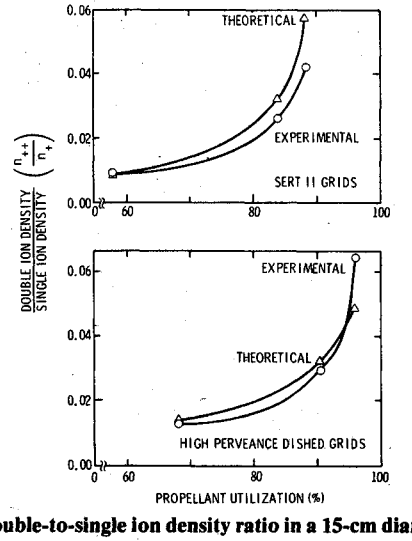

Fig. 3 Double-to-single ion density ratio in a 15-cm diam thruster.

Table 1 Data used for model verification and results

Operating Variables	Thruster Diameter (cm)	15.	15.	15.	15.	15.	15.	30.	30.	30.	30.	30.
	Grid Type	SERT II			HIGH PERVEANCE DISHED			EM	EM	EM	SHAG	SHAG
	Anode Current (I_{arc}--A)	1.0	1.7	2.05	3.02	4.06	4.13	5.0	7.5	10.0	9.5	11.7
	Anode Voltage (V_{arc}--V)	33.	37.2	42.6	32.2	37.5	40.4	37.	37.	37.	30.	30.
	Beam Current (I_{beam}--A)	.180	.258	.272	.499	.654	.622	1.0	1.5	2.0	1.5	2.0
	Mass Flow Rate (A)	.310	.307	.308	.735	.725	.650	1.25	1.76	2.29	1.74	2.30
Input Parameters	Plasma Volume to Surface Area Ratio (V/A--cm)	1.4	1.4	1.4	1.4	1.4	1.4	2.5	2.5	2.5	2.5	2.5
	Average Maxwellian Electron Temperature (T_{mx}--eV)	4.2	9.1	12.2	4.3	7.1	10.2	3.3	3.6	3.8	3.0	2.9
	Average Primary-to-Maxwellian Electron Density Ratio (n^*_{pr}/n^*_{mx})	.034	.083	.166	.017	.042	.134	.50	.35	.25	.19	.22
	Average Primary Electron Energy (ξ_{pr}--eV)	27.5	29.6	38.4	21.5	23.4	31.0	25.4	25.5	27.2	19.6	19.7
	Average Electron Density ($n^*_e \times 10^{-10}$ cm^{-3})	9.80	9.10	8.07	36.0	24.3	18.2	7.51	8.97	16.4	8.3	12.8
	Uniformity Factor F_+	2.3	2.1	2.3	2.0	1.9	1.8	1.5	1.5	1.5	1.8	1.7
	Uniformity Factor F_{++}	3.1	2.5	2.6	2.5	2.1	2.0	1.8	1.9	1.8	2.5	2.1
	Measured Double-to-Single Ion Current Ratio (I^{++}/I^+)	.024	.073	.12	.036	.081	.18	.080	.125	.167	.062	.080
Calculated Normalized Densities	Neutral Ground State Atoms	.63	.68	.73	.42	.50	.57	.71	.67	.58	.65	.59
	Neutral Metastable State Atoms	.12	.063	.040	.15	.086	.048	.060	.075	.085	.11	.11
	Neutral Resonance State Atoms	.21	.19	.14	.32	.28	.25	.14	.16	.19	.18	.22
	Singly Charged Ground State Ions	.036	.069	.084	.094	.12	.12	.081	.084	.13	.052	.076
	Singly Charged Metastable Ions	.002	.002	.002	.015	.011	.006	.003	.004	.010	.003	.006
	Doubly Charged Ground State Ions	.000	.002	.004	.002	.004	.007	.003	.003	.007	.001	.002
Calculated Production Fractions of Single Ions from	Neutral Ground State	.42(.39)[a]	.59(.23)	.70(.32)	.25(.17)	.40(.15)	.52(.29)	.66(.95)	.60(.91)	.52(.87)	.51(.87)	.47(.90)
	Neutral Metastable States	.29(.23)	.13(.19)	.08(.28)	.34(.10)	.19(.11)	.10(.25)	.12(.87)	.16(.79)	.19(.73)	.25(.69)	.24(.73)
	Neutral Resonance States	.29(.32)	.28(.22)	.22(.32)	.41(.13)	.41(.13)	.38(.28)	.22(.92)	.24(.87)	.29(.84)	.24(.78)	.29(.82)
Double Ions from	Neutral Ground State	.032(.26)	.15(.08)	.23(.31)	.012(0.)	.046(0.)	.09(.14)	.000(0.)	.000(0.)	.002(0.)	.001(0.)	.000(0.)
	Neutral Metastable States	.006(.26)	.014(.08)	.012(.31)	.004(0.)	.008(0.)	.008(.14)	.000(0.)	.000(0.)	.000(0.)	.000(0.)	.000(0.)
	Neutral Resonance States	.011(.26)	.040(.08)	.045(.31)	.009(0.)	.026(0.)	.039(.14)	.000(0.)	.000(0.)	.001(0.)	.000(0.)	.000(0.)
	Singly Charged Ionic State	.94(.62)	.78(.28)	.70(.35)	.95(.34)	.89(.21)	.84(.33)	.99(.99)	.99(.97)	.97(.95)	1.00(.95)	1.00(.97)
	Singly Charged Metastable Ionic States	.014(.72)	.013(.26)	.012(.41)	.025(.11)	.027(.07)	.022(.33)	.008(.99)	.010(.98)	.025(.97)	.001(.70)	.001(.76)

[a] Number in parentheses are the fraction of the indicated interactions effected by primary electrons.

temperature (T_{mx}) is seen to average approximately 9 eV over the primary electron region defined by the critical field line, whereas the primary electron energy (ξ_{pr}) averages about 30 eV. The average Maxwellian electron density (n_{mx}) is approximately 10^{11} cm^{-3}, whereas the average primary electron density (n_{pr}) is about 10^{10} cm^{-3} over the same region. electron densities and energies are seen to be fairly uniform in the primary electron region but drop off rapidly outside of this region. Using data similar to those plotted in Fig. 2 for each of the cases of Table 1, the volume-averaged properties and uniformity factors can be computed. The results of such a computation are presented in the "Input Parameters" section of Table 1, along with the volume-to-surface area ratio of the primary electron region (V/A) and the measured double-to-single ion current density ratio in the ion beam. The average values that resulted from an examination of Fig. 2 ($T_{mx} \simeq 9$ eV, $\xi_{pr} \simeq 30$ eV, $n_{mx} \simeq 10^{11}$ cm^{-3}, $n_{pr} \simeq 10^{10}$ cm^{-3}) are seen to agree with the volume-averaged values listed in Table 1 for the case listed in the second column ($T^*_{mx} = 9.1$ eV, $\xi^*_{pr} = 29.6$ eV, $n^*_{mx} = 8.4 \times 10^{10}$ cm^{-3}, $n^*_{pr} = 7.0 \times 10^9$ cm^{-3}). The uniformity factors F_+ and F_{++} are seen to have values of 2.1 and 2.5, respectively, for this case, and this implies that the single and double ion fluxes are 2.1 and 2.5 times as high in the bulk plasma as they are at the boundary defined by the screen grid and the critical field line. The average plasma properties listed in Table 1 are observed to cover a wide range in plasma conditions, a situation that is desirable for verification of the model.

The double-to-single ion density ratio inside of the discharge chamber, which is needed for comparison with the calculated value, can be determined from the measured ratio of the double ion current to the single ion current in the

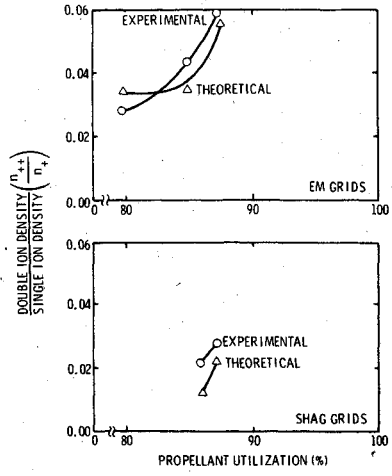

Fig. 4 Double-to-single ion density ratio in a 30-cm-diam thruster.

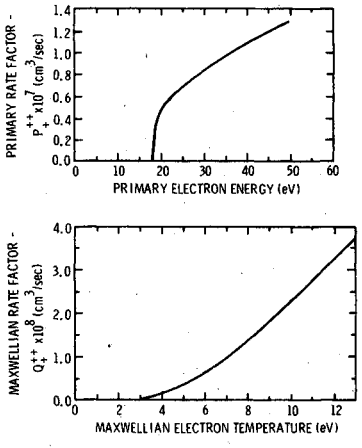

Fig. 5 Rate factors for $Hg^+ \rightarrow Hg^{++}$.

exhaust beam (I^{++}/I^+) through the equation

$$n_{++}/n_+ = I^{++}/(I^+ 2\sqrt{2}) \quad (1)$$

The quantity $2\sqrt{2}$ accounts for charge and Bohm criterion velocity differences between double and single ions. I^+ and I^{++} were measured at each point along a beam diameter using a mass spectrometer,[4] and a surface-area-averaged double-to-single ion current density then was computed from these data for inclusion in Table 1. The methods used for data acquisition and analysis using such a device are described in Ref. 11 for the 15-cm thruster data and in Ref. 8 for the 30-cm thruster. The ratio I^{++}/I^+ is, for example, equal to 7.3% for the 15-cm thruster, SERT II grid, 37-V anode voltage case, and the ratio is observed to increase with increasing input power to a given thruster.

Results and Discussion

The values of the average plasma properties, listed in Table 1, are observed to vary over large ranges. For example, the average Maxwellian electron temperature ranges from a low value of 2.9 eV to a high value of 12.2 eV. Similarly, the average primary-to-Maxwellian electron density ratio varies from 0.02 to 0.50. This large variation is considered sufficient to allow a general decision to be made about the suitability of the model for predicting the double-to-single ion density ratio in a thruster. The theoretical and experimental values of the double-to-single ion density ratio are plotted as a function of propellant utilization in Figs. 3 and 4. The "THEORETICAL" curves result from predictions made by the model using the "Input Parameters" listed in Table 1. The "EXPERIMENTAL" curves result from measurements of I^+ and I^{++} made using the mass spectrometer. The trends exhibited by the theoretical and experimental curves are very similar, and the theoretical and experimental values of the double-to-single ion density ratio generally agree to within 30%, although they differ by 40% for one case of a low double-to-single ion density ratio in the 30-cm thruster. These error values are considered to be acceptably small, considering the inherent errors in Langmuir probe analysis, and they suggest that the model is accurate over a wide range of plasma conditions and thruster configurations.

In view of the agreement in predicted and measured double-to-single ion density ratio, it is reasonable to expect that the species densities and relative production rates calculated in the model and used to predict the double-to-single ion density ratio also are accurate. Intermediate species densities and the relative production rates of double and single ions from these intermediate states as predicted by the model also are given in Table 1.

The section in Table 1 entitled "Calculated Normalized Densities" lists the model's predictions of the normalized densities of the states considered in this model. Normalized density of a species is defined here as the species density divided by the total heavy particle density (ions and atoms), and the sum of the normalized densities for any thruster condition therefore should equal unity. Table 1 shows, for example, that the 15-cm diam thruster operating with SERT II grids at 37-V anode voltage would be predicted to have 68% neutral ground state atoms, 19% neutral resonance state atoms, 6.9% singly charged ground state ions, and 0.2% doubly charged ground state ions. The normalized density of the single ions agrees fairly well in all cases with the 10% value quoted as typical of ion thruster plasmas in the literature.[12] As expected, the neutral ground state atoms are the most numerous.

The last section in Table 1 shows the calculated production rates for singly and doubly charged ions through the various intermediate states. These production rates have been normalized using the total production rate of the ionic species concerned. The fraction of the associated interactions affected by the primary electrons is indicated in parentheses. For example, at the 15-cm thruster's 37-V, SERT II grid operating point, 59% of the single ions are produced as a result of electron interaction with neutral ground state atoms, and 28% result from electron bombardment of neutral resonance state atoms. The neutral ground state to single ionic state interactions are induced by primary electrons 23% of the time and by Maxwellian electrons the remainder (77%) of the time.

Thruster performance is determined primarily by the mechanism for the production and loss of single ions. The production of these ions is, according to this model, quite dependent on the neutral metastable and neutral resonance states, which are ignored in most other analyses. The manner in which single ions are produced, however, differs a great deal between the two thrusters investigated here. In the 15-cm thruster, most of the single ions are produced as a result of Maxwellian electron bombardment, whereas primary electrons are relatively unimportant because of their low densities. This indicates that, for 15-cm thruster operation, the primary electron region is the important reaction region because it is the region where high densities of high-temperature Maxwellian electrons are found. In the 30-cm thruster, however, relatively high primary electron densities exist, and, since the Maxwellian electron temperature is low, most of the single ion production results from primary electron bombardment. So, for the 30-cm thruster, the primary electron region is the important reaction region because it contains high densities of high-energy primary electrons.

Table 1 indicates that in all cases a large percentage of the double ions are produced from single ions. This is as one would expect, because the minimum energy required to produce a double ion from a single ion is 18.7 eV, whereas 29

eV is required to produce a double ion from a neutral ground state atom. As the power input to the thruster increases, the number of electrons with energies greater than 29 eV increases, causing the relative importance of the neutral-to-double transition to increase. The lowest-energy path for the production of double ions is via the singly ionized metastable states, but the densities of these states are so low that this production mechanism is unimportant.

Simplified Model

Because most double ions are produced as a result of electron bombardment of single ions, other intermediate states for double ion production can be ignored with no significant loss in the accuracy of the double ion density calculations. Making this approximation, the doubly charged ion production rate is given by

$$R_{p^{++}} \simeq R_{p_+^{++}} = n_+^* [n_{pr}^* P_+^{++}(\xi_{pr}^*) + n_{mx}^* Q_+^{++}(T_{mx}^*)] \forall \quad (2)$$

where n_+^* is the volume-averaged single ion density, and $\forall$ is the primary electron region volume. $P_+^{++}(\xi_{pr}^*)$ is the primary electron velocity cross section product, defined by

$$P_+^{++}(\xi_{pr}^*) = v_e(\xi_{pr}^*)\sigma_+^{++}(\xi_{pr}^*) \quad (3)$$

In this equation, $v_e(\xi_{pr}^*)$ is the electron velocity corresponding to the energy ξ_{pr}^*, and $\sigma_+^{++}(\xi_{pr}^*)$ is the cross section[1] for the production of double ions from single ions at the electron energy ξ_{pr}^*. $Q_+^{++}(T_{mx}^*)$ is similar to $P_+^{++}(\xi_{pr}^*)$ but pertains instead to Maxwellian electrons and is given by

$$Q_+^{++}(T_{mx}^*) = \int_{E=0}^{E=\infty} \sigma_+^{++}(E) v_e(E) \frac{dn_{mx}(E)}{n_{mx}} \quad (4)$$

where $[dn_{mx}(E)/n_{mx}]$ is the Maxwellian distribution function pertaining to the temperature T_{mx}^*, and the other terms are as defined previously.

The total loss rate of double ions is given by

$$R_{l_{++}} = n_{++}^* v_{++}^* A / F_{++} \quad (5)$$

where n_{++}^* is the volume-averaged double ion density, v_{++}^* is the Bohm criterion doubly charged ion velocity,[5,13] A is the surface area of the primary electron region, and F_{++} is the doubly charged ion plasma uniformity factor.

Equating the loss and production rates and then solving the resultant equation for the double ion density, one obtains

$$n_{++}^* = n_+^* \frac{[n_{pr}^* P_+^{++}(\xi_{pr}^*) + n_{mx}^* Q_+^{++}(T_{mx}^*)] \forall}{v_{++}^* A / F_{++}} \quad (6)$$

The approximation $n_e^* = n_+^*$ ($n_e^* = n_{pr}^* + n_{mx}^*$) now can be used, and the Bohm criterion velocity for doubly charged ions can be substituted to obtain

$$n_{++}^* = n_e^{*2} \frac{\forall}{A} F_{++} \times \frac{[(n_{pr}^*/n_e^*) P_+^{++}(\xi_{pr}^*) + (n_{mx}^*/n_e^*) Q_+^{++}(T_{mx}^*)]}{[T_{mx}^* q (1 + n_{pr}^*/n_{mx}^*)/m_i]^{1/2}} \quad (7)$$

where q is the double ion charge (3.2×10^{-19} C), and m_i is the ion mass (kilograms).

The double ion density can be determined at a given thruster operation condition using this equation, the plots of the functions $P_+^{++}(\xi_{pr})$ and $Q_+^{++}(T_{mx})$ [defined by Eqs. (3) and (4)] found in Fig. 5, the volume-averaged plasma properties, and the uniformity factor F_{++}. This equation consistently will predict lower double ion densities than the complete model, since it ignores the production of double ions from neutral states and the singly ionized metastable states, but this error generally should be small. The error will be greatest for plasmas with high-energy electrons which can produce double ions directly from neutral states.

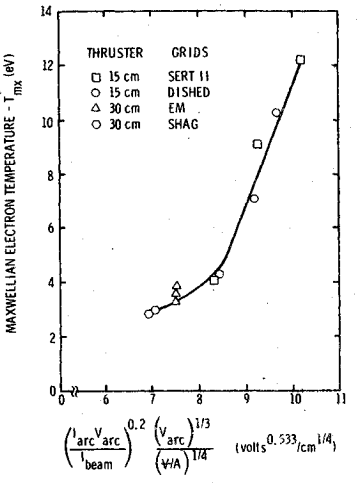

Fig. 6 Maxwellian electron temperature correlation.

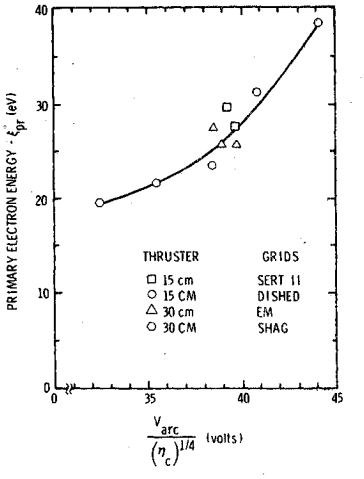

Fig. 7 Primary electron energy correlation.

The last section of Table 1 can be used to determine the magnitude of this error for the 11 cases considered in this study. Since the simplified model considers only the single-to-double transition, the error associated with this approximation can be determined from the listed value of the percentage of double ions produced from single ions. For example, for the 15-cm thruster, SERT II grids, 37-V anode voltage case, the percentage of double ions produced from single ions is 78%. This means that the value of the double ion density predicted by the simplified model would be 78% of that predicted by the complete model. Examination of Table 1 indicates that the double ion densities calculated using the simplified model will agree well with the complete model's predictions for all of the 30-cm thruster conditions, because, in these cases, the percentage of double ions produced from single ions is greater than 97%. In each of these cases, few electrons have energies in excess of 29 eV (the threshold energy for the neutral-to-double transition). The simplified model will, however, according to Table 1, yield results that are generally low for the 15-cm thruster data (e.g., 30% low for the SERT II grid, 42-V anode voltage condition) because, in these cases, sufficiently high Maxwellian electron temperatures exist to cause a relatively large percentage of the electrons to have energies in excess of 29 eV.

The most accurate way to determine the values of the average plasma properties required in Eq. (7) would be to make a Langmuir probe survey of the discharge chamber under consideration to determine the plasma properties at many different points and then to use this information to determine volume-averaged plasma properties and plasma uniformity factors. The collection of the plasma property

data is, however, costly and time-consuming. For this reason, average plasma property correlations have been developed. The correlating parameters used are composed of thruster operation parameters (e.g., arc current) and geometric properties (e.g., volume-to-surface area ratio of the primary electron region). Using the Maxwellian electron temperature data listed in Table 1, for example, one can obtain, through trial and error, the correlation presented in Fig. 6. The terms used in the correlating parameter are defined in Table 1.

The correlation for the primary electron energy shown in Fig. 7 contains the corrected propellant utilization (η_c). This parameter has been used instead of the measured propellant utilization because it resulted in a better fit of the data points. The propellant utilization (η) of an ion thruster, which is the ratio of beam ion current to beam ion and neutral current, depends upon the plasma properties, the effective open area for the loss of neutral atoms through the grids (A_0), and the effective open area for the loss of ions through the grids (A_+) in accordance with

$$\eta = \frac{n_+ v_+ A_+}{n_+ v_+ A_+ + n_{0t} A_0} \simeq 1 - \frac{n_{0t} v_0 A_0}{n_+ v_+ A_+} \tag{8}$$

In this equation, v_+ is the Bohm criterion velocity for singly charged ions,[13] v_0 is the thermal velocity pertaining to neutral atoms, and n_{0t} is the total neutral atom density. Primary electron energy can be correlated with the neutral-to-ion flux ratio ($n_{0t} v_0 / n_+ v_+$) that appears in this equation, but it does not appear to correlate with the ratio (A_0/A_+). For this reason, the corrected utilization in which the area ratio is held constant (at the value $[A_0/A_+]_{\text{std}}$) is used for correlation:

$$\eta_c = 1 - (n_{0t} v_0 / n_+ v_+)\,[A_0/A_+]_{\text{std}} \tag{9}$$

A convenient relationship between this corrected utilization and the conventionally defined utilization can be obtained by defining the standard area ratio and relating it to the area ratio of a given grid set. Equilibrium flow theory[12] indicates that the effective area for the loss of ions (A_+) from a thruster is proportional to the open area fraction of the screen grid (ϕ_s), and the effective open area for the loss of neutral atoms (A_0) is proportional to the quantity $(\phi_s \phi_a)/(\phi_s + \phi_a)$, where ϕ_a is the open area fraction of the accelerator grid. These two approximations can be used to define the ratio A_0/A_+ as

$$\frac{A_0}{A_+} = \frac{\phi_s \phi_a / (\phi_s + \phi_a)}{\phi_s} = \frac{\phi_a}{\phi_s + \phi_a} \tag{10}$$

Combining Eqs. (8-10), the following result is obtained:

$$\eta_c = 1 - 0.5(1-n)\,[(\phi_s + \phi_a)/\phi_a] \tag{11}$$

where the constant 0.5 has been used to define the standard grid set area ratio.

Figures 8-10 show correlations for the remaining input parameters. These correlations were developed by trial and error in a manner similar to that used to obtain those in Figs. 6 and 7. It should be noted that the correlation in Fig. 9 is for the quantity $n_{pr}^* [V/A]^{-1.5}$ rather than the primary electron density (n_{pr}^*).

Using the data of Figs. 5-10 and Eq. (7), a designer should be able to estimate the average doubly charged ion density in a divergent field thruster, and this will enable him to correct propellant utilization and thrust for doubly charged ions. The designer, however, also would like to know the peak doubly charged ion density occurring along the thruster centerline because it is this density that determines the peak erosion rates of the screen grid and baffle. The theoretical model utilizing volume-averaged plasma properties will not provide this information because it presumes uniform plasma conditions. The ratio of the doubly charged ion density on the thruster centerline to the average doubly charged ion density

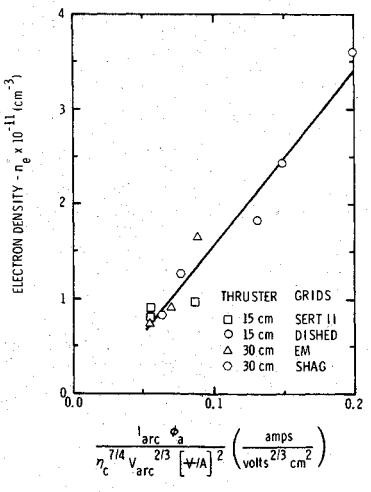

Fig. 8 Electron density correlation.

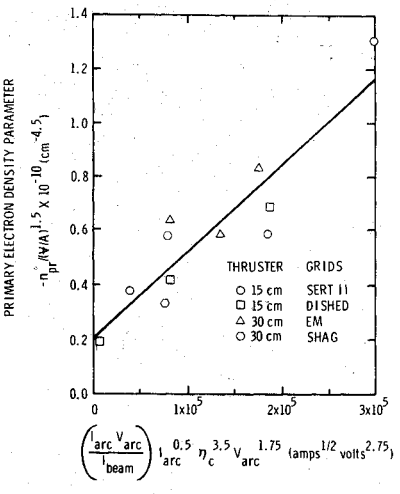

Fig. 9 Primary electron density correlation.

Table 2 Determination of the double ion density using the simplified model

Measured Thruster Variables
(15 cm thruster)

I_{arc} = 3. amps $\quad \phi_s$ = .67

V_{arc} = 32.2 volt $\quad \phi_a$ = .67

I_{beam} = .499 amps $\quad V/A$ = 1.4 cm

η = .68

Approximate Plasma Properties

T_{mx}^* = 4.6 eV $\quad n_{pr}^*$ = 5.3 x 10^9 cm^{-3}

ξ_{pr}^* = 22. eV $\quad n_e^*$ = 3.43 x 10^{11} cm^{-3}

F_{++} = 2.60 $\quad n_{mx}^* = n_e^* - n_{pr}^*$ = 3.38 x 10^{11} cm^{-3}

Calculation of the Double Ion Density

$$n_{++}^* = \frac{(3.43 \times 10^{11}\,\text{cm}^{-3})^2\,(1.4\,\text{cm})\,(2.60)}{[9.6 \times 10^9 \frac{\text{cm}^2}{\text{sec}^2\text{-eV}}\,(4.6\,\text{eV})\,(1.015)]^{1/2}}$$

$$\times [.015(.55 \times 10^{-7} \tfrac{\text{cm}^3}{\text{sec}}) + .985(.23 \times 10^{-8} \tfrac{\text{cm}^3}{\text{sec}}] =$$

6.3 x 10^9 cm^{-3}

(n_{++_ℓ}/n^*_{++}) can, however, be calculated from the measured doubly and singly charged ion current density profiles in the beam. Figure 11 shows this ratio (n_{++_ℓ}/n^*_{++}) plotted against a correlating parameter for the 15- and 30-cm diam thrusters.

As one might expect, the peak-to-average doubly charged ion density ratio correlates with the uniformity factor (F_{++}) for a given thruster configuration. The grid open area fraction ratio (ϕ_s/ϕ_a) facilitates correlation for thrusters of the same diameter having different grids. Figure 11 shows that the centerline-to-average doubly charged ion density ratio varies from 2.4 to 4.8 for the conditions and thrusters investigated in this study.

It should be understood that the correlations of Figs. 6-11 are based on data obtained from divergent magnetic field thrusters. The average plasma properties predicted using these figures may be inaccurate for other types of thrusters (e.g., multipole or radial field thrusters). Langmuir probe surveys should be made for these other types in order to obtain good estimates of the average plasma properties and hence accurate predictions of the average double ion density.

Application of the simplified model can be demonstrated best through an example. Consider a 15-cm thruster operating at the conditions defined by the first section of Table 2. The corrected utilization (η_c) first is calculated using Eq. (11), and a value of 68% is obtained. Next, the correlating parameters are calculated. For example, the value of the correlating parameter

$$\left[\frac{I_{\rm arc}V_{\rm arc}}{I_{\rm beam}}\right]^{0.2}\frac{(V_{\rm arc})^{1/3}}{(V/A)^{1/4}}$$

used in Fig. 6 is 8.4 $V^{0.533}/cm^{1/4}$. This value indicates that the average Maxwellian electron temperature would be 4.6 eV.

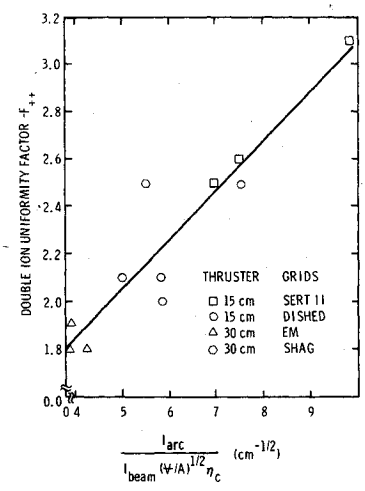

Fig. 10 Uniformity factor correlation.

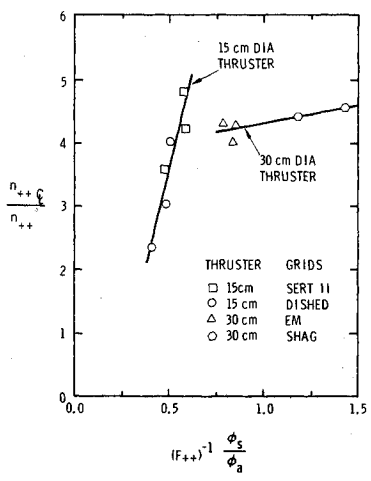

Fig. 11 Peak-to-average doubly charged ion density ratio correlation.

The remainder of the average plasma properties were determined in a similar manner. The results obtained are listed in the second section of Table 2. Using the values of the average primary electron energy and the average Maxwellian electron temperature obtained from Figs. 6 and 7, one can enter Fig. 5 and determine P_+^{++} (22 eV) $= 0.55\times10^{-7}$ cm^3/sec and Q_+^{++} (4.6 eV) $= 0.23\times10^{-8}$ cm^3/sec. These quantities, together with the average densities, the uniformity factor, and the volume-to-surface area ratio for this thruster, then are substituted into Eq. (7) to obtain the double ion density, as shown in the last section of Table 2. The double ion density calculated using the simplified model is 6.3×10^9 cm^{-3}, whereas the value calculated using the complete model is 5.2×10^9 cm^{-3}. The major reason for the discrepancy is the higher electron temperature (4.6 eV) obtained from Fig. 6 than that used by the complete model (4.3 eV). This causes $Q_+^{++}(T^*_{mx})$ to be too large and results in the overestimate of the average double ion density.

To estimate the peak doubly charged ion density, Fig. 11 is entered using the correlating parameter value ($F_{++}^{-1}\,\phi_s/\phi_a = 0.40$) to obtain the peak-to-average density ratio of 2.4. Using this value, the peak doubly charged ion density would be 1.5×10^9 cm^{-3}.

Theoretical Trends

Equation (7) indicates some general trends that should be considered in the design and operation of electron bombardment thrusters. For example, the double ion density varies linearly with the volume-to-surface area ratio; therefore, if two thrusters have the same average plasma properties, the larger thruster will have a higher double ion density. Equation (7) suggests that double ion density reductions could be achieved readily by reducing the electron density, which appears as a squared term. Making arbitrary adjustments in the plasma properties to reduce the double ion density may, however, have an adverse effect on other aspects of thruster performance which also must be considered. An examination of the effect of electron density on propellant utilization will indicate one of the effects that such an adjustment would have. The propellant utilization previously defined in Eq. (8) is

$$\eta = 1 - \frac{n_0^* v_0 A_0/A_+}{n_+^* v_+} \tag{8a}$$

The single ion density (n_+^*) can be approximated by the electron density (n_e^*), and Kaufman[14] has shown that neutral density (n_0^*) varies inversely with the volume-to-surface area ratio of the discharge region.

With these substitutions, Eq. (8a) becomes

$$\eta = 1 - \frac{A_0/A_+}{n_e^* \forall/A} f(T^*_{mx}, \xi^*_{pr}, \frac{n^*_{pr}}{n^*_{mx}}, F_+) \tag{12}$$

where f is a function of the quantities indicated. From this equation, one can see that reducing the electron density to reduce the double ion density also will have the undesirable effect of reducing the propellant utilization. However, if geometrical changes in thruster design accompany the reduction in the electron density, the propellant utilization can be held constant while the double ion density is reduced. For example, a thruster having twice the volume-to-surface area ratio of its predecessor could be operated at one-half the electron density to effect the same propellant utilization while exhibiting half of the double ion density in accordance with Eq. (7).

It also might be desirable to reduce the double ion density of a thruster having a given size while maintaining the same propellant utilization. In this case, the propellant utilization could be held constant by reducing both the ratio A_0/A_+ (which reduces the relative escape rate of neutrals) and the electron density so that their ratio was constant. According to

Eq. (7), this would result in a large reduction in the double ion density, which varies directly as the square of the electron density. The data in Table 1 for the two 30-cm thruster configurations at 1.5 and 2.0 A beam current show that this is an effective means of reducing double ion density without reducing propellant utilization, as the only difference in these two thruster configurations is the open area fraction of the accelerator grid. The EM accelerator grid has an open area fraction (ϕ_a) of 45%, whereas the open area fraction for the SHAG accelerator grid is 23%. Both sets have a 69% open area fraction for the screen grid. The value of the ratio A_0/A_+ can be calculated, using Eq. (10), to be 0.39 for the EM grids and 0.25 for the SHAG grids. The change from EM grids to SHAG grids then allowed operation at a given propellant utilization to occur at a lower arc voltage and hence at lower electron densities and energies and, therefore, at lower double ion densities.

Conclusions

A discharge chamber model for an electron bombardment ion thruster has been developed which considers metastable, resonance, and ground state atomic and ionic production and loss mechanisms. The model can be used to predict doubly charged ion densities from plasma property information. These calculated double ion densities generally agree with measured values to within 30%. Correlations, which relate average plasma properties to thruster operating variables such as anode current, can be used to estimate the average plasma properties in divergent magnetic field thrusters when the properties themselves are not available. Singly charged ions are produced, according to this analysis, in significant numbers in two-step processes through intermediate metastable and resonance states, in addition to direct ionization from the neutral ground state. Doubly charged ions are produced predominantly via the singly ionized ground state, with direct ground state neutral-to-double ion production becoming more significant in plasmas with high Maxwellian electron temperatures (>5 eV) and primary electron energies (>29 eV). A simplified model, which considers only the singly ionized ground state in double ion production, can be used to predict double ion densities that agree with the complete model's predictions to within about 10% when primary electron energies and Maxwellian electron temperatures are less than 29 and 5 eV, respectively. The recent experimental observation[9] that the use of small-hole accelerator grids in conjunction with lower anode voltages provides a means for reducing double ion densities in thrusters, without degrading performance, is supported by the model.

Acknowledgment

This research was supported by NASA under Grant NGR-06-002-112 and Contract NAS3-19703.

References

[1] Peters, R.R., "Double Ion Production in Mercury Thrusters," NASA CR-135019, April 1976.

[2] Peters, R.R. and Wilbur, P.J., "Double Ion Production in Mercury Thruster," AIAA Paper 75-398, New Orleans, La., March 1975.

[3] King, H.J. et al., "2½ KW Low Specific Impulse, Hollow Cathode Mercury Thruster," AIAA Paper 69-300, March 1969.

[4] Vahrenkamp, R.P., "Measurement of Doubly Charged Ions in the Beam of a 30 cm Mercury Bombardment Thruster," AIAA Paper 73-1057, Lake Tahoe, Nev., Oct. 1973.

[5] Wilbur, P.J., "Hollow Cathode Restartable 15 cm Diameter Ion Thruster," NASA CR-134532, Dec. 1973.

[6] Bechtel, R.J., Cskiy, G.A., and Byers, D.C., "Performance of a 15 cm Diameter Hollow Cathode Kaufman Thruster," AIAA Paper 68-88, New York, Jan. 1968.

[7] Poeschel, R.L., King, H.J., and Schneider, D.E., "An Engineering Model 30 cm Thruster," AIAA Paper 73-1084, Lake Tahoe, Nev., Oct. 1973.

[8] Poeschel, R.L. et al., "2.5 Kw Advanced Technology Ion Thruster," NASA CR-134687, Aug. 1974.

[9] Poeschel, R.L. et al., "High Power and 2.5 Kw Advanced Technology Ion Thruster," Hughes Research Labs., Malibu, Calif., Monthly Rept. 7, Contract NAS 3-19703, Jan. 1976.

[10] Beattie, J.R., "Numerical Procedure for Analyzing Langmuir Probe Data," *AIAA Journal*, Vol. 13, July 1975, pp. 950-952.

[11] Wilbur, P.J., "15 cm Mercury Ion Thruster Research," NASA CR-134905, Dec. 1975.

[12] Kaufman, H.R., "Technology of Electron Bombardment Ion Thrusters," *Advances in Electronics and Electron Physics*, Vol. 36, edited by L. Marton, Academic Press, New York, 1974, pp. 265-373.

[13] Masek, T.D., "Plasma Properties and Performance of Mercury Ion Thrusters," *AIAA Journal*, Vol. 9, Feb. 1971, pp. 205-212.

[14] Kaufman, H.R., "Ion Thruster Propellant Utilization," NASA TN D-6591, Dec. 1971, p. 16.